Available online at www.sciencedirect.com

jmr&t Journal of Materials Research and Technology

www.jmrt.com.br

Original Article

Application of hybrid nature-inspired algorithm: Single and bi-objective constrained optimization of magnetic abrasive finishing process parameters

Atul Babbar[a], *Chander Prakash*[b], *Sunpreet Singh*[c], *Munish Kumar Gupta*[d], *Mozammel Mia*[e], *Catalin Iulian Pruncu*[e,f,*]

[a] *Department of Mechanical Engineering, Thapar Institute of Engineering and Technology, Patiala, India*
[b] *Mechanical Engineering, Lovely Professional University, Phagwara, India*
[c] *Mechanical Engineering, National University of Singapore, Singapore*
[d] *Key Laboratory of High Efficiency and Clean Mechanical Manufacture, Ministry of Education, School of Mechanical Engineering, Shandong University, Jinan 250061, China*
[e] *Mechanical Engineering, Imperial College London, Exhibition Rd., SW7 2AZ London, UK*
[f] *Mechanical Engineering Department, University of Birmingham, Birmingham B15 2TT, UK*

ARTICLE INFO

Article history:
Received 20 November 2019
Accepted 1 May 2020

Keywords:
Firefly algorithm
Magnetic abrasive finishing
Material removal rate
PSO
Surface characteristics

ABSTRACT

The manufacturing quality generated by the magnetic abrasive finishing (MAF) of brass depends of some critical process variables. Therefore, in this survey were investigated the optimization of this process taking into account the material removal rate and surface characteristics using a hybrid nature inspired algorithm (particle swarm optimization (PSO) coupled with firefly algorithm (FA)). In the initial step, the design matrix was generated using the Taguchi L16 orthogonal array, thereafter, obtaining the experimental protocol for developing the MAF process. The regression analysis was confronted with the analysis of variance (ANOVA) simulations to facilitate determination of the percentage contribution of each input parameters. The influence of individual and combined process parameters investigated via standard PSO, FA, and hybrid HPSO-FA were used for mono and bi-objective constrained optimization. This innovative way of processing the brass plate revealed that machining time was the most dominant parameter which contributed maximum towards variation in response variables determined.

Crown Copyright © 2020 Published by Elsevier B.V. This is an open access article under the CC BY-NC-ND license (http://creativecommons.org/licenses/by-nc-nd/4.0/).

1. Introduction

Over recent decades, it was noted that the traditional machining processes are not able to fulfill the demands of increasingly growing manufacturing industries. These processes are under

* *Corresponding author.*
E-mail: c.pruncu@imperial.ac.uk (C.I. Pruncu).
https://doi.org/10.1016/j.jmrt.2020.05.003
2238-7854/Crown Copyright © 2020 Published by Elsevier B.V. This is an open access article under the CC BY-NC-ND license (http://creativecommons.org/licenses/by-nc-nd/4.0/).

a lot of pressure because they need to generate complex shapes and implementing innovative designs to manufacture products with desired tolerances and interchangeability. Some conventional machining processes like grinding, honing, lapping, boring shaping, and milling etc., have major limitation due to high stresses which in turn generate surface damage and poor topography. This entail specific attention on the state-of-art, with keen interest to innovative manufacturing methods able to produce parts with high dimensional tolerances and perform machining with great performances not only on harder materials but also on soft and ductile ones [1]. A suitable method to solve this issue is the magnetic abrasive finishing (MAF). It permits to remove the extra material from the work-piece surface using the abrasive particle activated by the magnetic field. The MAF allows an evenly distribution of the magnetic abrasive particles over work-piece surface. The magnetic field is controlled by a high load that activates the magnetic activity, in which the abrasive material arranges them in a particular fashion depending upon magnetic field lines. Hence, it forms a structure that is known as magnetic abrasive brush (MAB) which is flexible in nature. This multipoint cutting tool acts as an indenter and strives the work-piece surface with certain pressure. There, the abrasion is the main phenomenon describing the material removal during the MAF process [2,3].

Recently, major developments have been made to enhance the surface finish of different materials with MAF strategy. In [4], authors outlined an improvement in the surface morphology by applying the MAF process, while processing the stainless steel 202 material. The importance of each parameter on the output response was detected by Taguchi L_9 orthogonal array. It was concluded that high surface finish can be attained by using the optimum size of abrasive particles. In another investigation [5], authors outlined the behavior of flexible magnetic abrasive brush during MAF of a single disk and double disk experiments. A comparison was made for machining with a permanent magnet and without the magnet. It was observed that surface texture significantly improved by using permanent magnets. On same context, Kala et al. [6] established a surface roughness model in double desk MAF process. Further, Kala and Pandey [7] detected the optimum results by optimization of MAF with the following parameters: the mesh size 1200, feed rate of 1 mm/min, working gap of 2.3 mm, the abrasive weight percentage of 36%, and spindle speed of 467 rpm. On the other hand, Li et al. [8] produced a better surface morphology where the levels of the optimized process parameters are dictated by the spindle speed (600 rpm), mesh size (320) combined with the mixing ratio that is 4:3:1.

The MAF process is considered a viable alternative for practical aspects is specific modern applications. It has been observed that there are several research efforts made on MAF process by considering various process parameters. However, we noted no research was conducted on the brass plate using MAF process to enhance their surface morphology. This motivates to explore in depth this research and fill this gap. Therefore, the present investigation were focused to detect the great potential played by the MAF in order to obtain better surface roughness, considering as a case study the brass plate submitted to Iron-boron bonded abrasives. The brass is selected because of its high usability in various sorts of industrial applications. The high strength properties, good ductility, and better corrosion resistance in harsh conditions make it suitable for low-speed axial piston pump. In this application the cylinder barrel made of brass is always in sliding contact with the port plate and to achieve superior sliding condition is required bets surface quality. Currently, coarse and fine grinding is utilized for the machining of the port plate [3]. These conventional methods are not able to make the surface free defect; therefore, it enables high wear during operation of the pump. This leads to reduced efficiency and life-span of the pump. In that reason, were further optimized the process parameters developed by the MAF process that are crucial to reduce the cost and processing time. There are numerous numbers of techniques such as Taguchi's methodology, response surface methodology, and genetic algorithm, and particle swarm optimization techniques used for the optimization of manufacturing process parameters [9–17], but they have different limitation in convergence time, results accuracy and so on. For example, the main problem associated with conventional Taguchi method is that it cannot be used for optimization of multi-objective problems [18–26]. In this direction, the process parameters during MAF of brass were optimized with hybrid algorithms i.e., particle swarm optimization method (PSO) coupled with firefly algorithm [27]. The major benefits of these algorithms are that they are easily used for any type of constrained or un-constrained problems. Here, the feasibility of integration of PSO with firefly algorithm (FA) has been introduced to predict the optimal conditions of MAF parameters. The efficacy of the hybrid PSO-FA (HPSOFA) is compared with PSO and FA optimization technique. The effect of MAF input process parameters (spindle speed, the amount of magnetic abrasives, and size of mesh together with machining duration) on the surface roughness (R_a) and materials removal rate (MRR) was studied. The quality of surface finish which was improved due to the optimization process developed, revealed by using the field-emission scanning electron microscopy (SEM) and atomic force microscopy (AFM).

2. Materials and methods

2.1. *Abrasives preparation*

The brass plate was chosen for the present study and abrasives were prepared by a sintering process. Firstly, iron powder (mesh size 300) was poured into a die along with boron carbide powder (mesh size 280) in the mixing ratio of 85:15. The iron and boron carbide powder were initially mixed. Then, the homogeneous mixture obtained was compressed in a hydraulic press using a static load of 200 MPA for cc. 20 s. The die surface lubrication was ensured by applying a layer of freshly prepared slurry of zinc stearate containing methanol. Hence, the produced compacts were carefully located into heating tube of a furnace for sintering. After sintering, compacts were crushed to get abrasive particles of different mesh size. Fig. 1 depicts the complete experimental procedure.

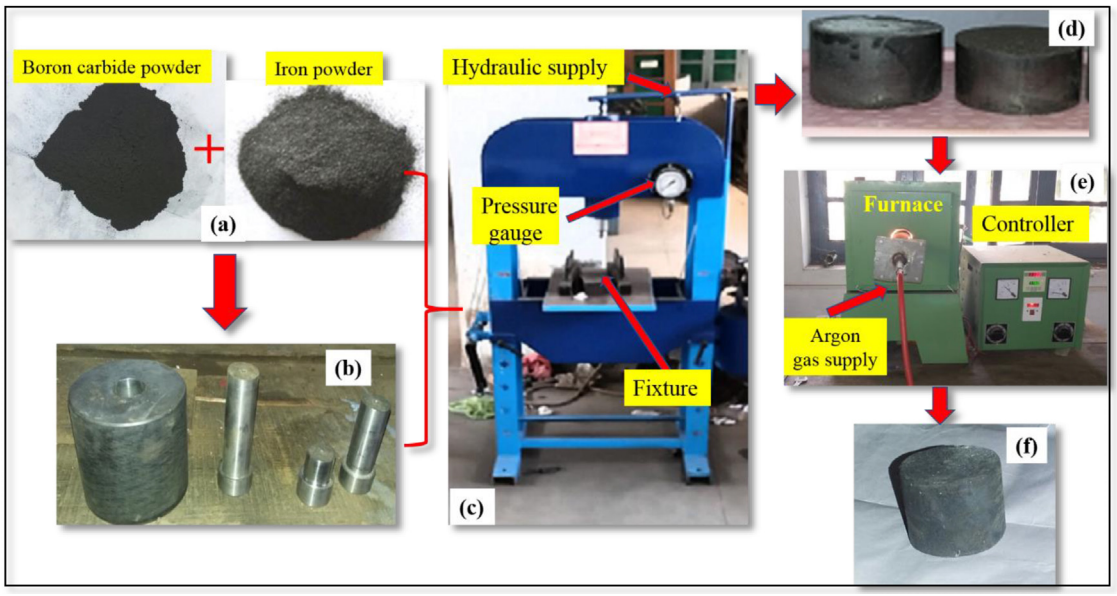


Fig. 1 – Steps involved in the preparation of bonded magnetic abrasives: (a) mixing of iron powder and boron carbide powder, (b) die, plunger, stopper, and punch, (c) hydraulic press, (d) compacts after compaction, (e) sintering furnace, and (f) sintered compacts.

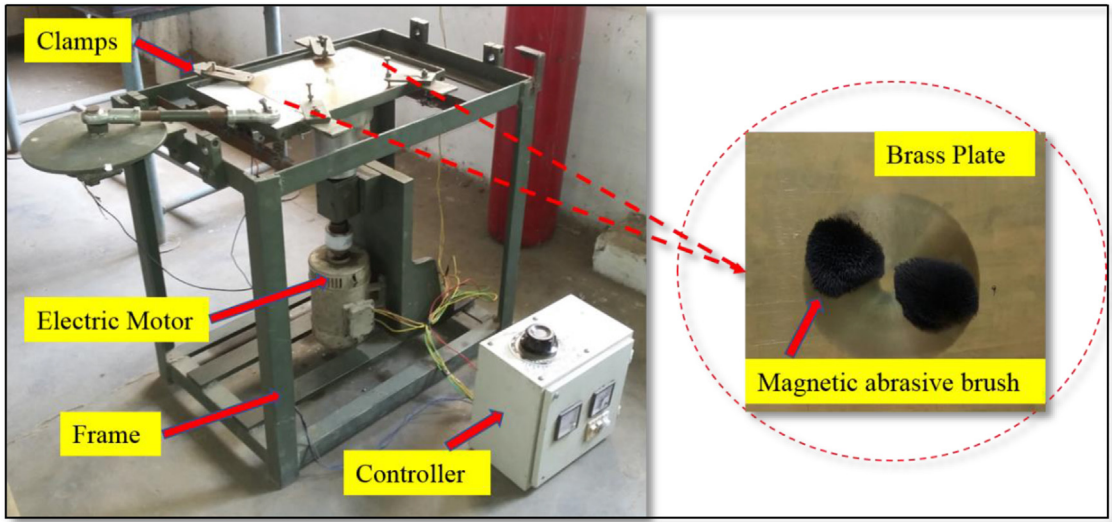


Fig. 2 – Experimental setup with different components.

2.2. *Settled of procedure*

Fig. 2 shows the experimental set-up of MAF process. There, the two magnets (5000 Gauss each) were mounted on an aluminum chuck which was coupled to a shaft connected to the motor. A specific controller was used in order to control the motor speed (rpm). It has an inbuilt step-down transformer to command the input current voltage.

In the above configuration, the workpiece was placed upon a support made from acrylic material. The reason for choosing acrylic material for support is that it is non-magnetic in nature and it remains inert under the influence of applied magnetic field. Four clamps were used at four ends to restrict the movement of the workpiece during the finishing process. Table 1 summarizes the different levels selected for experiments. A Taguchi L16 orthogonal array system was employed for experimentation and parameters were selected on the basis of literature survey. The input parameters (i.e. speed of spindle (rpm), the amount of abrasives (mg), the size of mesh size together with time of machining (sec)) allows to detect the effect on R_a while achieving the maximum MRR. For validation each test was produced at least three times that further permits to avoid any possibility of error.

Initially, the roughness of the surface was measured at pre-selected points randomly on the workpiece. The workpiece was positioned just above the rotating magnetic chuck. The working gap was kept 20 mm which was selected after trail experimentation to ensure proper magnetic abrasive brush. The abrasives made were poured over the workpiece. Further, the magnetic field was activated to move the micro-

Table 1 – Control log of experimentation.

Input Parameters	Symbol	Low level (–)	High level (+)
Spindle speed (rpm)	A	100	200
Quantity of magnetic abrasives (mg)	B	5	10
Mesh number	C	140	270
Machining time (min)	D	30	60

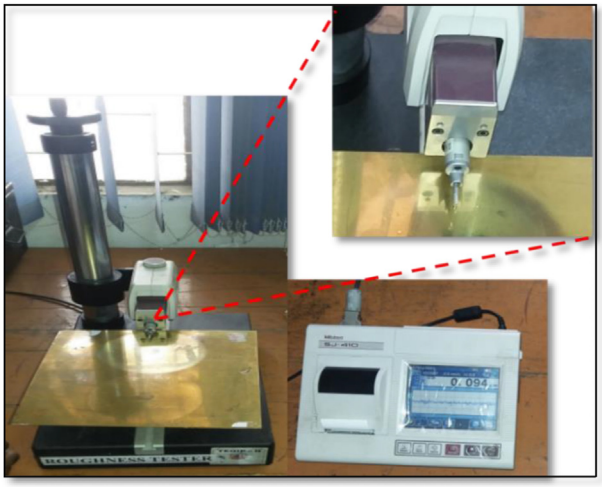


Fig. 3 – The R_a tester (Model:SJ-410, Make: Mitutoyo).

cutting adhesive edges in order to removes the material from workpiece surface. With the progression of machining time, irregularities present on the surface were smoothened. Mitutoyo SJ-410 based R_a tester was again used to check the change in roughness value at same pre-checked points, as exhibits in Figs. 3 and 4.

In order to determine the MRR was measured the workpiece weight before and after MAF process and its numerical equation were introduced in Eq. (1):

$$MRR = (W_b - W_a)/t_m \quad (1)$$

where, W_a, W_b, and t_m are workpiece weight in the initial state, workpiece weight at the end of MAF process, and MAF processing duration, respectively. Fig. 5 shows comparative surface topography of raw sample (a, b) and MAF processed sample (c, d).

3. Outline of hybrid nature-inspired algorithms

In this section, the outline of implemented algorithms is presented in very well manner. The details are furnished below:

3.1. *Particle swarm optimization (PSO)*

The PSO approach can be classified as an evolutionary method that is based on the swarm and population [18], suitable for predicting highly reliable results [19]. The roots of this technique are connected with the behavior of birds, fish, and other swarms which do not have any colonial leader. As in such swarms animals find their food and preys, randomly, and gradually they achieve the best condition for potential solution, similarly, in PSO, the optimal solution is attained through random iterations of the involved scenario. The PSO was devel-

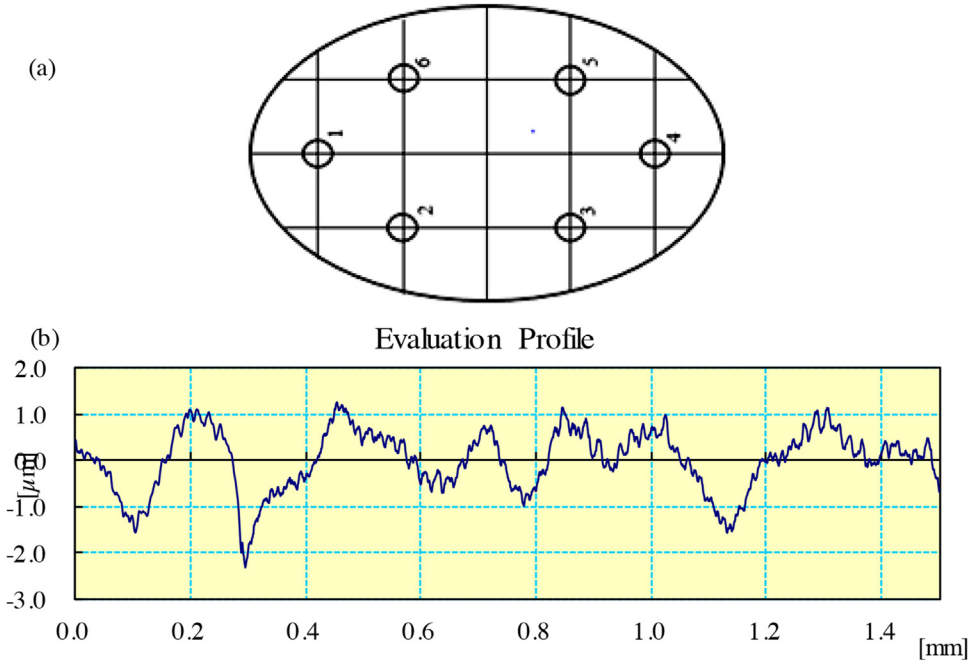


Fig. 4 – Ra measurements: (a) observation points on the finished workpiece and (b) a digitized surface roughness plot.

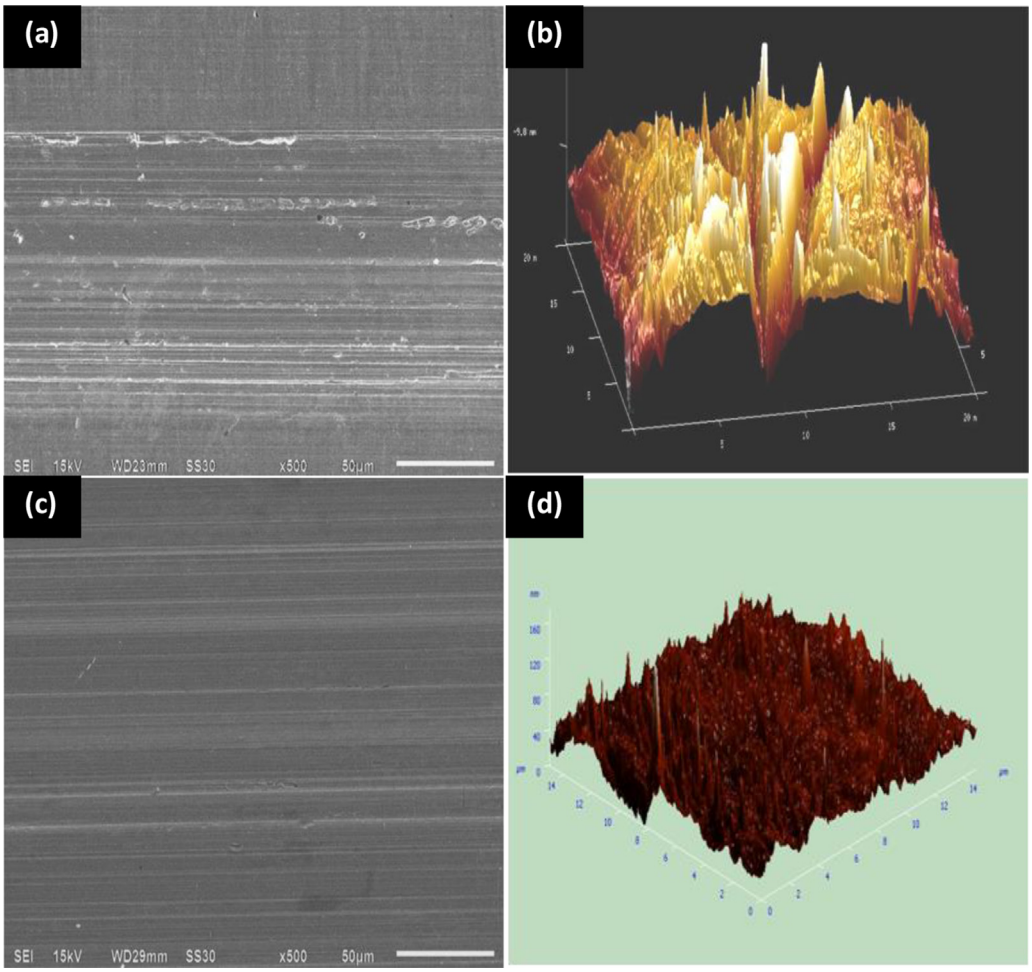


Fig. 5 – SEM and FFM image before (a, b) and after MAF finishing (c, d).

oped around two decades ago by a social psychologist and an electrical engineer, Kennedy and Eberhart, respectively, who exploited the simple analogues of social interaction. The very first simulation, presented in 1995, was influenced by a previously reported work on analogues of bird flocks searching for corn [20]. The PSO works on a couple of entities, or particles, that are placed within the space of search of an issue or area of concern in order to evaluate the objective of the search at parent location. Afterwards, each and every particle generates a specific path in the search space guided by a combination between the current history best-fitness positions with random perturbations [20]. This is followed by the iteration to relocate all particles, and, consequently, the swarm is most probable to locate near of an optimum of the fitness, described by Eq. (2) and (3):

$$v_{i,j}(t+1) = wv_{i,j}(t) + c_1 r_1 \left(pb_{i,j} - x_{i,j}(t)\right) + c_2 r_2 \left(pb_{g,i} - x_{i,j}(t)\right),\ j = 1, 2, \ldots d \quad (2)$$

$$x_{i,j}(t+1) = x_{i,j}(t) + v_{i,j}(t+1),\ j = 1, 2, \ldots d \quad (3)$$

where, c_1 & c_2 represents as coefficients values, inertia factor is denoted by w, r_1 and r_2 termed as random variables having value of [0,[1]]. In comparison of the non-linear, multimodal optimization, and non-differentiable methods, PSO is fast and robust [22]. Despite the existing enormous benefits, such as ease to use, speed to get the results, and broad coverage, the practical utility of this method is still limited. The continuous nature of PSO makes it unsuitable for combinatorial problems. To remedy this drawback, it can be used, successfully, in combination of FA.

3.2. *Firefly algorithm (FA)*

The FA method is very attractive. It is build using the multimodal functions and have a structured approach that is more efficient [23]. The FA method is basically based on idealizing the flashing behavior of fireflies [24–26]. This includes three basic rules as follows:

- Unisex consideration: All fireflies are considered of same sex and are assumed they attract another firefly.
- Proportionality: The attractiveness is linked to the brightness which is proportional to each other. Any pair of flashing fireflies indicates the firefly arrangements that connect the less bright with the brighter one.
- Objective landscape: The objective function field could be affected by the brightness intensity and is sensitive to maximization problems case; therefore, the brightness should be proportionally to the objective function's value.

Here, these bio-luminescence processes are answerable for flashing light of fireflies. In the case of firefly algorithm were detected that the pattern of these rhythmic flashes are quite unique generated on rhythm of flashes, flashing rate and as well as are associated with the period of time for which flashes [24,25]. They reproduce the natural algorithm structure attraction of mamifer species in which a male is attracted by a female. This algorithm is described by an inverse square, given as Eq (4):

$$I\alpha 1/r2 \tag{4}$$

Where, I and r are the light intensity and intermediate distance, respectively. The environment has an absorbent role while the intensity of light decrease for larger distance. These parameters produce limitation for fireflies when they want to communicate during the night, therefore they need few hundred of meters during the night to well communicate with each other.

3.3. *Hybrid particle swarm optimization firefly algorithm (HPSOFA)*

The HPSOFA allows achieving a precise and reliable outcome during computation of special functions [8]. In this process, it is necessary to establish a quite fast convergence speed target on the early period once the iterations start. It has been reported by various authors that classical PSO strategy provides the fastest convergence ability when compared to others for the same type of problems. PSO have some convergence limitation when require matching the local search database to the global resolution. There, the control between exploration and exploitation is dictated by some specific PSO parameters: weight of inertia (w) and coefficients of acceleration ($c1$, $c2$) [2]. In thus system, the particle velocity (V) is determined by using Eq. (2). They are significant in local search, are thereafter used for evaluating the position of the next particles. However, determination with accuracy of velocity is highly difficult for local search because a small perturbation generates particles oscillation that leads within delays for the optimization strategy. To avoid this challenge the velocity is not considered in exploitation stages. The advantage of considering in the FA permits to simulate the process without the velocity (V) characteristic. Moreover, in case of firefly algorithm, there is no need to use parameter from anterior best position for each firefly. Hence, it allows a free movement for the fireflies [27].

In the present work, hybrid optimizations have been used combining the ability of firefly search with the PSO strategy [27]. It leads to strength prediction due a suitable balance between the exploration and exploitation. This combination uses the maximum from PSO that will generate the global search, and highly convergence potential in exploration, whereas, FA will manage to overcome the issue of local search with better option for exploitation. This process was proved to be usefully when its inertia weight is adjusted during dynamic simulation by well detecting the previous personal best. First of all, the various selected parameters are used by both algorithms. They are used as pre-defined search in specific velocity range that is generated randomly from uniform particle vectors. They further allow calculate the global (g_{best}) and personal best (p_{best}) of the particles with specific assignments. To detect if the particles position was improved in its fitness value were used the Eq. (5) for this iteration. The new position is saved as temp variable. Their position and its velocity were determined using Eq. (6) to Eq. (8).

$$w = w_i - ((w_i - w_f)/iteration_{maximum}) \times iteration \tag{5}$$

$$f(i,\ t) = \left\{ \begin{array}{l} true,\ if\ fitness\ \left(particle_i^t\right) \le gbest^{t-1} \\ false,\ if\ fitness\ \left(particle_i^t\right) > gbest^{t-1} \end{array} \right\} \tag{6}$$

$$x_i(t+1) = x_i(t) + B_0 e^{-\gamma r^2 ij}(x_i(t) - gbest^{t-1} + a \in_i \tag{7}$$

$$V_i(t+1) = V_i(t+1) - X_{i_temp} \tag{8}$$

A better position of the particles in respect to its previous global best is driven by the FA, otherwise its progress is managed by the PSO; in the latter case a standard procedure occurs that is based on Eq. (2) and Eq. (3). When the maximum limit is reached (in terms of iteration), the hybrid algorithm stops whereas the g_{best} and its *fitness* value are considered the results of novel hybrid strategy.

4. Results and discussion

The end of experiments produces results considered outputs responses that are recorded and plotted. Table 2 presents the responses measured and achieved in this hybrid simulation.

4.1. *Statistical tests*

A numerical software MINITAB-17 was used to determine the influence of each parameters and its interaction outcomes on determined parameters from the process (R_a and MRR). The corresponding models were shown by Eq. (9) and Eq. (10).The regression models, hence developed were used to predict the response for different process parameters and results were further optimized by using subjected algorithms [28,29].

Regression model for Ra:

$$\begin{aligned} Ra =\ & 0.3250 - (0.10750 \times A) - (0.00300 \times B) - (0.05650 \times C) \\ & - (0.02850 \times D) + (0.00100 \times A \times B) + (0.02300 \times A \times C) \\ & + (0.01700 \times A \times D) + (0.00100 \times B \times C) - (0.00300 \times B \times D) \\ & - (0.00700 \times C \times D) \end{aligned} \tag{9}$$

Regression model for MRR:

$$\begin{aligned} MRR =\ & 3.699 - (0.020 \times A) + (0.570 \times B) - (0.805 \times C) \\ & - (1.123 \times D) - (0.0675 \times A \times B) + (0.0825 \times A \times C) \\ & + (0.0275 \times A \times D + (0.1125 \times B \times C) - (0.1925 \times B \times D \\ & + (0.1375 \times C \times D) \end{aligned} \tag{10}$$

Table 2 – Measure output responses with their parameter levels.

Experiment No.	Input process parameters				Output parameters	
	A	B	C	D	Ra (μm)	MRR (mg/min)
1	100	5	140	30	0.161	2.41
2	100	5	140	60	0.14	1.25
3	100	5	270	30	0.12	1.92
4	100	5	270	60	0.096	1
5	100	10	140	30	0.158	2.9
6	100	10	140	60	0.133	1.48
7	100	10	270	30	0.121	2.47
8	100	10	270	60	0.085	1.26
9	200	5	140	30	0.097	2.5
10	200	5	140	60	0.089	1.3
11	200	5	270	30	0.079	2.04
12	200	5	270	60	0.066	1.05
13	200	10	140	30	0.09	2.7
14	200	10	140	60	0.086	1.55
15	200	10	270	30	0.076	2.58
16	200	10	270	60	0.063	1.32

Tables 3 and 4 presents the values determined using analysis of variance (ANOVA) simulation that permits to indicate the role of each process parameter for the output responses. It simply distributes the deviation of response variable within sample means. This technique was exploited to check any significant difference among groups mean as well as to quantify the contribution of process parameters towards the output [30–32]. The contribution of the error was less than 5% which shows highly accurate and precise results were obtained. The value of R^2 shows that our data is highly correlated. It is clear from the Fig. 6 that machining time contributes more to the variation in response characteristics in comparison to the other parameters.

4.2. *Responses and their impact*

The process parameters implication to the end responses has been investigated in two manners: (1) Individual effect (2) Interaction effect. The descriptions of these effects are furnished below:

4.2.1. R_a

Individual effect produced by the rotational speed: The R_a in dictate by the variation of embedded speed. A higher speed permits to reduce the roughness as were noted when it vary from level 1–2 (see Fig. 6). The higher rotational speed can enlarge more magnetic abrasive particles to create a homogenous surface finish. They produce shearing of surface peak generating higher surface finish. Instead, when a lower rotational speed were used it was detected a less centrifugal force acting on the magnetic abrasive particles. Therefore, the particles were located near of the center of MAF process providing a less accurate brush mechanism [4].

Individual effect derived from the abrasives quantities: Fig. 6 present the results achieved when was increased the magnetic abrasive amount. They seem to have detrimental effect on the surface roughness when the amount of abrasive is higher. It could because the higher mixture numbers/size of abrasive that will come in contact with workpiece surface.

Individual effect as per mesh number: The R_a is greatly affected by mesh number of the abrasive particles. As the mesh number increased (i.e. from level 1 to level 2), there slight decrease in surface roughness was observed (see details of Fig. 6). Bigger the mesh number means smaller abrasive particle size, which provides small cutting power and leads to low abrasiveness; thus results in better surface finish. On the other hand, smaller mesh number means large abrasive particle size, which provides large cutting power and leads to high abrasiveness; thus results in poor surface finish.

A finer abrasives particle generates a better surface finish whereas the coarse abrasives generate significantly lower surface finish. Therefore, a higher mesh number can entail more cutting edges during the machining of workpiece surface.

Individual effect associated to machining time: Fig. 6 indicates a better surface finish when a longer period of machining process was embedded. As long as it was increasing the machining time from level 1–2 there was possible to achieve a better surface finish. The consistent magnetic abrasive that is generated on the workpiece surface allows creating a smooth and even material surface activated by the continuously work of the sharp cutting edges during this longer process.

Interaction effect linked to combination of rotational speed and mesh number: Fig. 7(a) presents the evolution of interaction plots that combine the rotational speed and mesh number to detect the effect on R_a. The mean of R_a is reduced by increasing the rotational speed (i.e. from level 1 to level 2). The level 2 mesh number abrasives (270 mesh) produce a better R_a in respect to level 1 size abrasives (140 mesh). The increase of speed permits to reduce the gap of a mean R_a values. Further, when the rotational speed and mesh number are increased simultaneously the R_a decreases (see Fig. 7(a)). The level 1 indicates a higher R_a values (dark green) while the level 2 was detected a superior R_a (blue color).

Interaction effect linked to combination of rotational speed and machining time: Fig. 7(b) presents the evolution of interaction plots that combine the rotational speed and machining time to detect the effect on R_a. It is appreciable that the R_a is reduced by the increment in the rotational speed. The R_a was detected bigger on the level 1 while the level 2 of

Table 3 – AVOVA for R_a values.

Source	Degree of freedom	Sum of sqaure	Variance	Fisher's value (F value)	Probability (P value)
Regression	10	0.014602	0.001460	219.17	0.000*
A	1	0.001643	0.001643	246.59	0.000*
B	1	0.000001	0.000001	0.17	0.699
C	1	0.000472	0.000472	70.89	0.000*
D	1	0.000106	0.000106	15.95	0.010*
A*B	1	0.000001	0.000001	0.08	0.783
A*C	1	0.000541	0.000541	81.14	0.000*
A*D	1	0.000281	0.000281	42.11	0.001*
B*C	1	0.000002	0.000002	0.23	0.649
B*D	1	0.000011	0.000011	1.59	0.267
C*D	1	0.000046	0.000046	6.84	0.047*
Error	5	0.000033	0.000007		
Total	15	0.014635			

Model Summary

S	R^2	R^2(adj)	R^2(pred)
0.0025812	99.77%	99.32%	97.67%

* represents significant terms.

Table 4 – ANOVA for MRR values.

Source	Degree of freedom	Sum of sqaure	Variance	Fisher's value (F value)	Probability (P value)
Regression	10	6.95945	0.698945	13948.9	0.000*
A	1	0.00215	0.002146	42.92	0.001*
B	1	0.07011	0.070113	1402.25	0.000*
C	1	0.07354	0.157810	1470.87	0.000*
D	1	0.15751	0.000100	3156.20	0.000*
A*B	1	0.00010	0.000025	2.00	0.216
A*C	1	0.00002	0.002025	0.50	0.511
A*D	1	0.00202	0.001325	40.50	0.001*
B*C	1	0.00123	0.070225	24.50	0.004*
B*D	1	0.07022	0.044100	1404.50	0.000*
C*D	1	0.00025	0.000050	882.00	0.000*
Error	5	0.00025			
Total	15	6.98970			

Model Summary

S	R^2	R^2(adj)	R^2(pred)
0.0070711	99.98%	99.96%	97.95%

* represents significant terms.

machining time produce a lower R_a. The increase of speed permits to reduce the gap of a mean R_a values curves. Further, when the rotational speed and machining time are increased simultaneously the surface roughness decreases (see Fig. 7(b)). The level 1 indicates a higher R_a values (dark green) wile in the level 2 was detected a superior R_a (blue color).

Interaction effect linked to combination of mesh number and machining time: Fig. 7(c) presents the evolution of interaction plots that combine the mesh number and machining time to detect the effect on R_a. The R_a is reduced by the increment in the rotational speed (from level 1 to level 2). The average value of the R_a was detected bigger on the level 1 while the level 2 of mesh number produce a lower Ra. The level 2 machining time (60 min) produce a better R_a in respect to level 1 time (30 min). The increase of mesh number permits to reduce the gap of a mean Ra values curves. Further, when the mesh number and machining time are increased simultaneously the R_a decreases (see Fig. 7(c)). The level 1 of mesh number indicates a higher R_a values (dark green) wile in the level 2 was detected a superior R_a (blue color).

4.2.2. MRR

Individual effect produced by the rotational speed: Fig. 8 present indicates the rotational speed has a direct effect with it was increased. Such as, by increasing the speed were detected slightly higher MRR. Once the hitting process with the abrasive occurs in a more repetitive action the workpiece interface becomes softened (lower interface hardness) that is leading larger amount of MRR.

Individual effect derived from the abrasives quantities: The MAF process generates higher MRR when the abrasive material was increased as quantity from 5 to10 gm (see Fig. 8). This is associated to large amount of abrasive that get in contact with the workpiece and strike it, therefore producing more material to be eliminated.

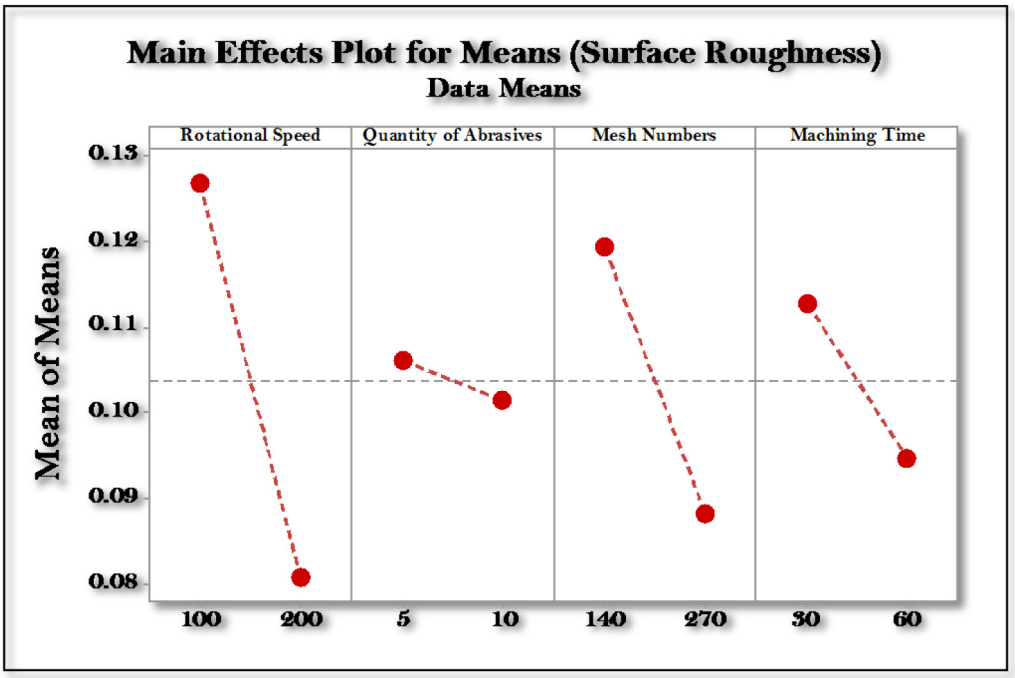


Fig. 6 – Main effects plot for means of R_a.

Individual effect as per mesh number: As per Fig. 8, it was noticed that when a bigger mesh number were used they generate a lower MRR. Seems that coarse abrasives require large area of contact (i.e. less contact pressure) and the workpiece interface resist better to striking contact that prevent material to be detached. The small mesh generates abrasive particles which produces higher contact pressure when they hit the workpiece interface. It enables to overcome the material yielding point paving the possibility to produce higher MRR.

Individual effect associated to machining time: Fig. 8 reveals that the decreases by using a long machining time. This progress is associated to abrasives that can get blunt, such as their cutting capacity reduces. There the particles density may decreases as per a mixture with the material broken from workpiece that transforms into adhesive powder. The adhesive powder material grain can suffer some changes leading to a less consistent material which further decreases the MRR.

Interaction effect linked to combination of rotational speed and machining time: Fig. 9(a) presents the evolution of interaction plots that combine the rotational speed and machining time to detect the effect on MRR. The mean of MRR is increased by increasing the rotational speed (i.e. from level 1 to level 2). The mean of the MRR were detected lower on the level 1 while the level 2 of rotational speed produce higher MRR. The level 1 machining time (30 min) produce a bigger MRR in respect to level 2 time (60 min). Further, when the speed and machining time are increased simultaneously the MRR increases (see Fig. 9(a)).The level 1 of machining time indicates a higher MRR values (dark green) while in the level 2 was detected a less MRR (blue color).

Interaction effect linked to combination of mesh number and quantity of abrasives: Fig. 9(b) presents the evolution of interaction plots that combine the mesh number and quantity of abrasives to detect the effect on MRR. The mean of MRR is increased by increasing the quantity of abrasives (i.e. from level 1 to level 2). The mean of the MRR were detected higher on the level 1 mesh number while the level 2 of mesh number produce lower MRR. Further, when the quantity of abrasive was increased and the mesh number decreased simultaneously the MRR increases (see Fig. 9(b)). The level 2 of quantity of abrasive indicates a higher MRR a value (dark green) while in the level 2 was detected a less MRR (light green color).

Interaction effect linked to combination of quantity of abrasives and machining time: Fig. 9(c) presents the evolution of interaction plots that combine the quantity of abrasives and machining time to detect the effect on MRR. The mean of MRR is increased by increasing the quantity of abrasives (i.e. from level 1 to level 2). The mean of the MRR were detected higher on the level 1 while the level 2 of machining time produce lower MRR. Further, when the quantity of abrasive was increased and machining time decreased simultaneously the MRR increases (see Fig. 9(b)). The level 2 of quantity of abrasive indicates a higher MRR values (dark green) while the level 2 was detected a less MRR (dark blue color).

Interaction effect linked to combination of mesh number and machining time: Fig. 9(d) presents the evolution of interaction plots that combine the mesh number and machining time to detect the effect on MRR. The mean of MRR is reduced by increasing the mesh number (i.e. from level 1 to level 2). The mean of the MRR were detected higher on the level 1 while the level 2 of mesh number produce lower MRR. Further, when the quantity of mesh number was decreased and machining time decreased simultaneously the MRR increases (see Fig. 9(d)). The level 1 of mesh numberindicates a higher MRR values (dark green) while the level 2 was detected a less MRR (dark blue color).

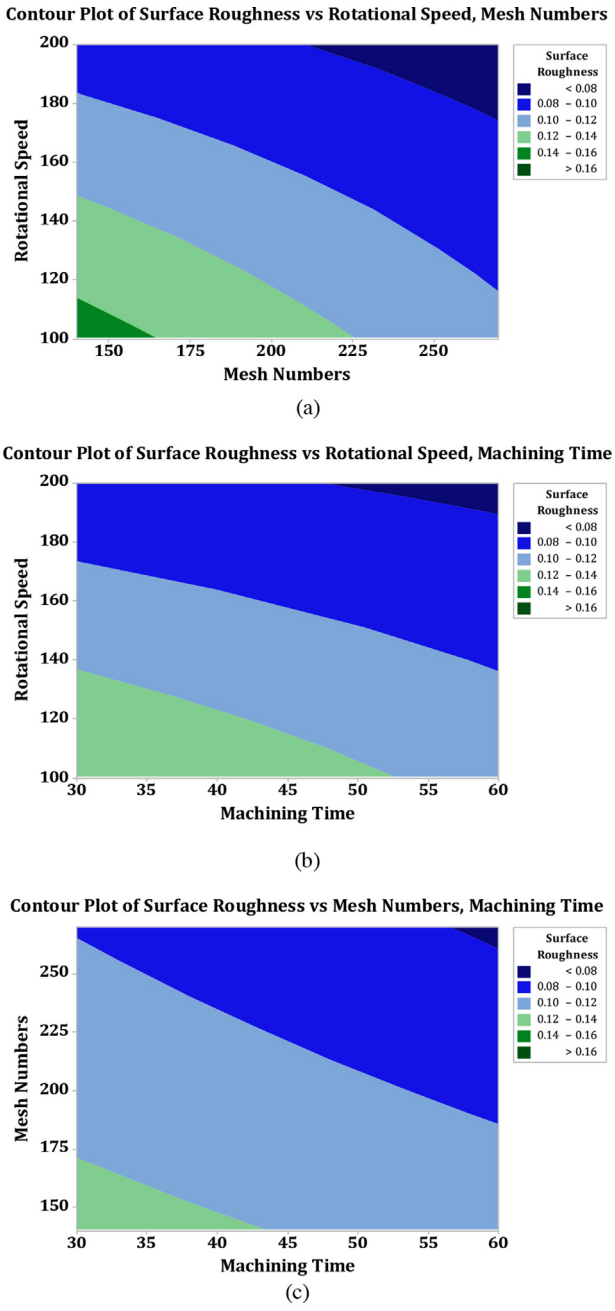


Fig. 7 – Interaction effect plots for R_a: (a) rotational speed vs. mesh number (b) rotational speed vs. machining time (c) mesh numbers vs. machining time.

4.3. *Process parameters optimization by PSO, FA, and HPSOFA*

The process optimization developed on the MAF was conducted twofold: (1) by optimization of a single objective constrained and (2) bi-objective constrained optimization method. The first one was designed to obtain the individual optimal global solution achieving best R_a value associated to a maximum MRR value. The second algorithm has been performed in the bi-objective optimization method. In this regard, initially the algorithms parameters were decided ad the fitness function has been inserted in the MATLAB code. After that, the optimization model has been developed and the algorithm is verified with the help of confirmation experiments. The method of selecting initial learning parameters followed by details of single and bi-objective constrained optimization is presented in the sub sequent sections.

4.3.1. *Generation of learning parameters*

The implemented algorithm needs some specific learning parameters in order to run the MATLAB program. For instance, W_{max}, W_{min} C1 and C2 are the major learning parameters that explore the performance of PSO algorithm. However, the firefly algorithm is parameter-free algorithm that means it does not

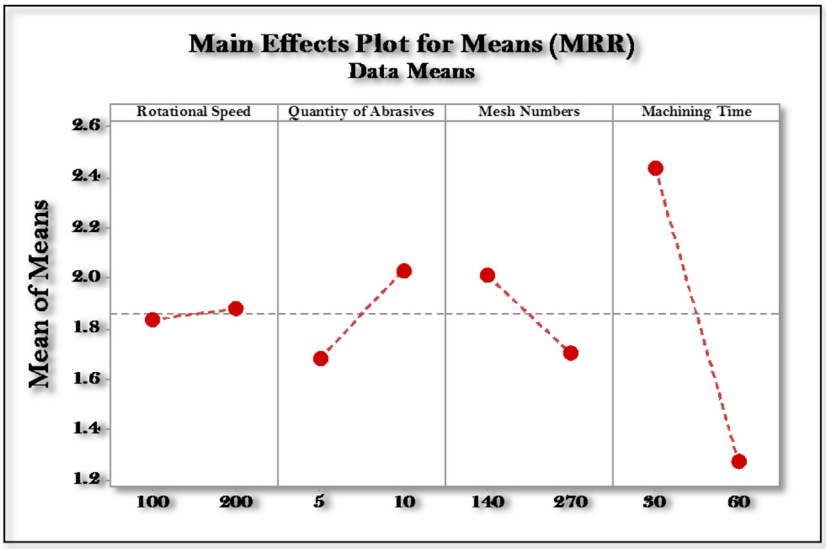


Fig. 8 – Main effects plot for means of MRR.

Table 5 – Initial parameters of PSO and HPSOFA.

Input parameters	Value of parameters
S, number of agent particles	50
Number of iterations	100
Maximum permissible inertia weight	1.4
Minimum permissible inertia weight	0.5
Maximum defined learning rate, $C1_{max} = C2_{max}$	2
Minimum defined learning rate, $C1_{min} = C2_{min}$	1.5
H	5

require any initial learning parameters for the efficient running of the program. The vital learning parameters that were used in the case of PSO and HPSOFA are presented in Table 5. The credibility of these parameters were mostly depends upon the practitioner's knowledge and literature survey [8,33–36].

4.3.2. *Single and bi-objective optimization strategy to improve the process parameters*

The first one (single optimization) were developed to obtain the individual optimal global solution achieving best R_a value associated to a maximum MRR value. The constrained or boundary conditions were used as per the following criteria:

Spindle speed: 100–200 rpm, amount of magnetic abrasives: 5–10 mg, the mesh size/number: 140–270 and duration of machining: 30–60 min

Then, the fitness function is required to run the MATLAB code of subjected algorithms. Therefore, in the single objective optimization, the individual equations generated through regression equations are used as the fitness function for MATLAB code. Then, the code is run at 100 iterations and the optimum values have been obtained with the application of these algorithms. The optimal values obtained through optimization methods are tabulated in Table 6. Further, Figs. 10 (a) and (b) presents the convergence characteristics graph of each factor. The best optimal parameters to obtain low R_a (0.058 μm) are 210 rpm spindle speed, 12 mg magnetic abrasives, 270 mesh size and 60 min duration of machining, respectively. Furthermore, when it used the spindle speed of 100 rpm, the amount of magnetic abrasives 10 mg, mesh size of 140 during a duration time of 30 min were obtained the optimal parameter setting for maximize the MRR.

Table 6 – Control variables and their selected values (for optimal response variables).

Control variables	Optimal values for response variables								
	Ra (μm)			MRR (gm/min)			Combined Values		
	PSO	FA	HPSO-FA	PSO	FA	HPSO-FA	PSO	FA	HPSO-FA
Spindle speed (rpm)	200	200	210	100	100	100	200	200	210
Quantity of magnetic abrasives (mg)	10	10	12	10	10	10	10	10	11
Mesh number	270	270	270	140	140	140	270	270	270
Machining time (min)	60	60	60	30	30	30	30	30	30
Best Solution	0.062	0.061	0.058	2.84437	2.7423	2.98532	1.074	1.0652	1.0127
Standard deviation	0.856	0.754	0.423	0.762	0.712	0.354	0.983	0.854	0..473
Average time (sec)	14.02	6.04	4.08	14.02	6.04	4.08	14.02	6.04	4.08
Success rate	80%	82%	95%	80%	82%	95%	80%	82%	95%
Percentage error	8.034	7.08	4.01	7.56	6.82	3.21	8.43	7.42	4.08

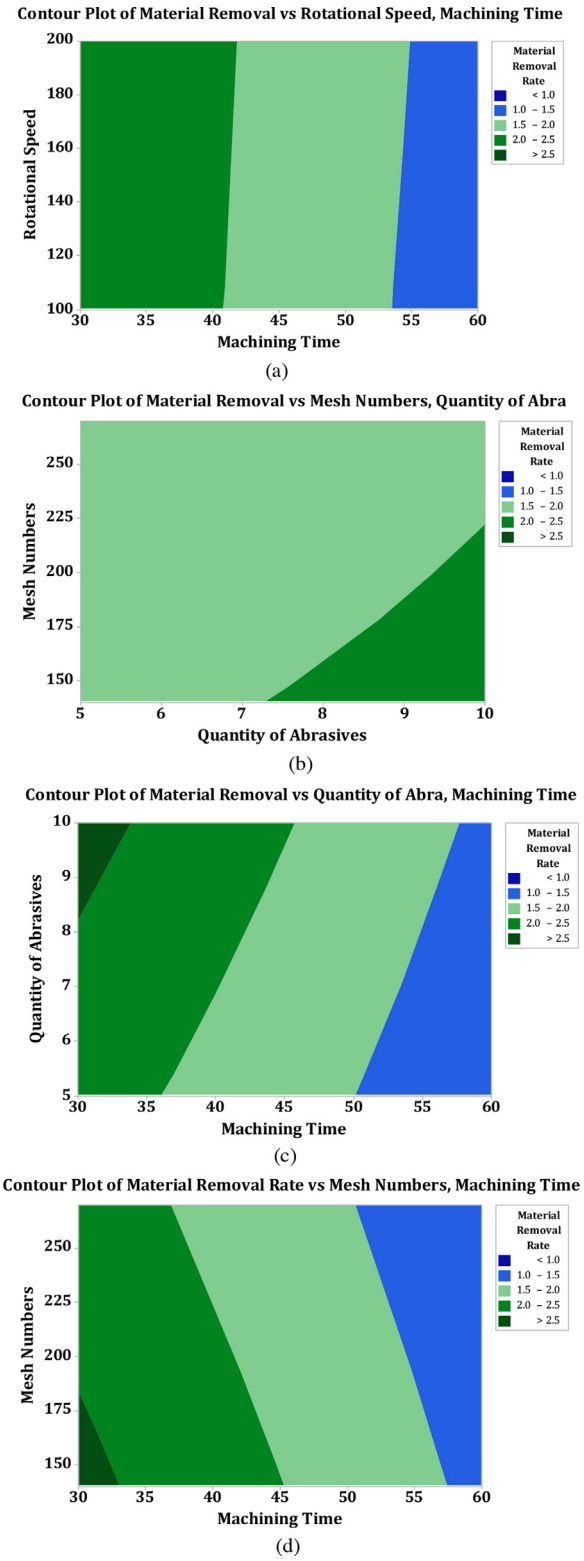


Fig. 9 – Interaction effect plots for MRR: (a) rotational speed vs. machining time, (b) mesh numbers vs. quantity of abrasives, (c) quantity of abrasives vs. machining time, and (d) mesh numbers vs. machining time.

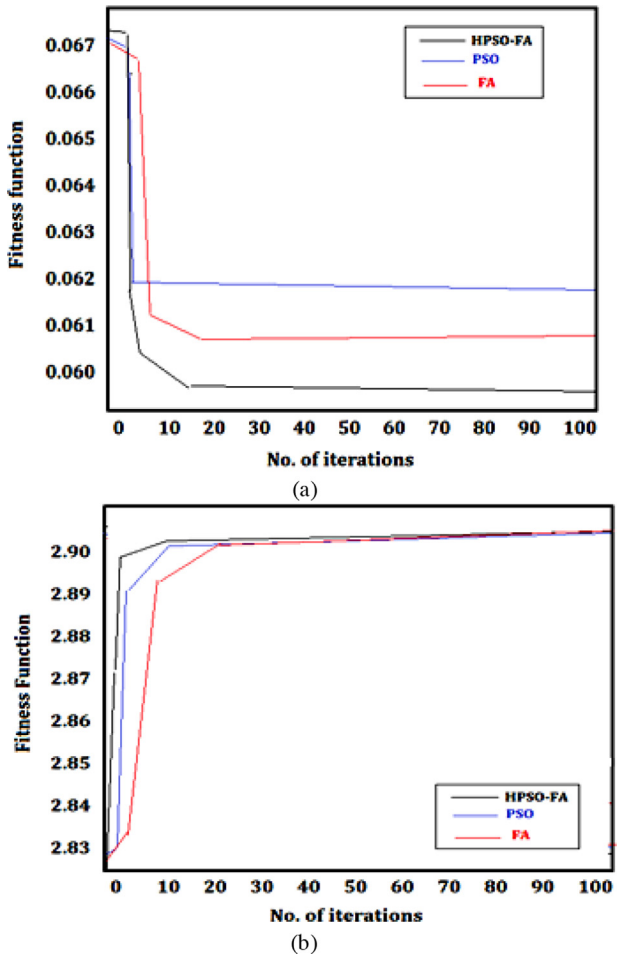


Fig. 10 – Convergence characteristics graphs for single objective optimization: (a) minimum R_a value and (b) maximum MRR value.

While using bi-objective optimization were developed a combined objective solution. For establishment of combined objective function three theories has been considered (1) Maximization of responses (2) Minimization of responses and (3) Grouping of minimization and maximization. In the present work, the combination of minimization and maximization criterion is used to evaluate the objective function because the target were superior R_a (as low as possible values) values with a maximum MRR values. Hence, for evaluating the combined function, following Eq. (11) is used.

$$Z_{\min} = \frac{W_1 * Z_1}{Z_{1\,\min}} + \frac{W_2 * Z_2}{Z_{2\,\max}} \tag{11}$$

where, Z_{1min} = *Minimum Ra value,* Z_{2max} *is maximum MRR value,* W_1 & W_2 *represents each* weight allocated to the responses, i.e., 0.50 for each response. Further, the identical constraints, boundary conditions and calculated combined function Z_{min} are used in the MATLAB program for minimized bi-objective optimization. From the formulated results (as shown in Table 6 and Fig. 11), it has been noted that the 210 rpm spindle speed, 11 mg magnetic abrasives, 270 mesh number and 30 min

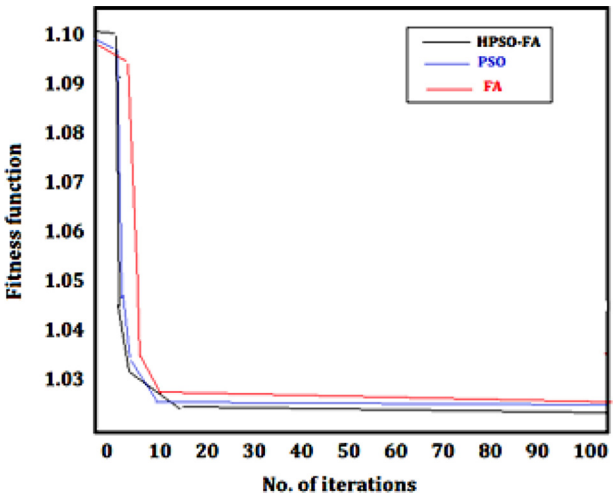


Fig. 11 – Convergence characteristics graphs for bi-objective optimization of combined objective.

machining time is the optimal parameter for minimized combined objective values i.e., 1.0127.

Lately, the comparison of optimal results for single and bi-objective optimization is made between the standard PSO, FA, and HPSO-FA, as given in Table 6. From these comparison results, it has been interestingly noticed superior outcomes from the hybrid HPSO-FA in respect to the standard PSO or/and FA. According to the optimized results, it has been found that the error and standard deviation values are less in the case of HPSO-FA with low computational time of 4.08 s. This is due to the fact that the application of HPSO-FA tried to mitigate the premature convergence and local optima solution. Moreover, the integration of both processes increases the calculation ability of PSO and consequently the proper balancing between exploration and exploitation stage has been take place. Besides, the HPSO-FA increases the searching ability of PSO because the population gets advanced and only is oriented to detect the best personal and global particles, before it reaches to the termination criterion [27].

5. Conclusion

The present paper demonstrates the application of hybrid nature inspired algorithms for optimization of MAF process parameters. The optimization is successfully applied in two ways (1) Single objective (2) Bi-objective. The investigation of process parameters has been made in order to identify the best Ra at the expenses of maximum MRR values developed during the MAF routine. The conclusions drawn from the present investigation has been listed below:

- The results from this survey demonstrated the robustness of HPSO-FA that represents a versatile optimization method as compared with the standard PSO and FA. It significantly improves the contribution of MRR to a maximum limit but in mean time offer the best surface characteristic for the Ra during the MAF process.
- The effect of different process parameters (i.e. speed of spindle, abrasives amount, size of mesh and duration of machining) reveals that the duration of machining is the most critical parameter for the quality characteristics. The size of mesh, speed of spindle and abrasives amount is succeeding as importance.
- By using specific regression models was possible to create a strong relationship that connect the input parameters with their predictors. These computational models were further utilized for the prediction of output response variables.
- The optimal parameters that offer the best results for Ra (0.058 μm) are: 210 rpm spindle speed, 12 mg abrasives amount, 270 size of mesh and 60 min duration of machining, respectively. Furthermore, the 100 rpm spindle speed, 10 mg abrasives amount, 140 size of mesh and 30 min duration of machining are the optimal parameters as setting which can produces the maximum MRR.
- By using the followings parameters: 210 rpm spindle speed, 11 mg magnetic abrasives, 270 mesh number and 30 min machining time enable to obtain the optimal parameter for minimizing the combined objective values i.e., 1.0127.

Conflict of interest

The authors declare no conflicts of interest.

REFERENCES

[1] Chang GW, Biing-Hwa Y, Rong-Tzong H. Study on cylindrical magnetic abrasive finishing using unbonded magnetic abrasives. Int J Mach Tools Manuf 2002;42:575–83.
[2] Wu J, Yanhua Z, Hitoshi S. Study on ultra-precision magnetic abrasive finishing process using low frequency alternating magnetic field. J Magn Magn Mater 2015;386:150–9.
[3] Zhu Y, Chen X, Zou J, Yang H. A study on the influence of surface topography on the low-speed tribological performance of port plates in axial piston pumps. Wear 2015;338:406–17.
[4] Ahmad S, Gangwar S, Yadav PC, Singh DK. Optimization of process parameters affecting surface roughness in magnetic abrasive finishing process. Mater Manuf Process 2017;32:1723–9.
[5] Kala P, Pandey PM, Verma GC, Sharma V. Understanding flexible abrasive brush behavior for double disk magnetic abrasive finishing based on force signature. J Manuf Process 2017;28:442–8.
[6] Prateek P, Sharma V, Pandey PM. Surface roughness modelling for double disk magnetic abrasive finishing process. J Manuf Process 2017;25:37–48.
[7] Prateek K, Pandey PM. Comparison of finishing characteristics of two paramagnetic materials using double disc magnetic abrasive finishing. J Manuf Process 2015;17:63–77.
[8] Li W, Li X, Yang S, Li W. A newly developed media for magnetic abrasive finishing process: material removal behavior and finishing performance. J Mater Process Technol 2018;260:20–9.
[9] Prakash C, Kansal HK, Pabla BS, Puri S. Multi-objective optimization of powder mixed electric discharge machining parameters for fabrication of biocompatible layer on β-Ti alloy using NSGA-II coupled with Taguchi based response surface methodology. J Mech Sci Technol 2016;30(9):4195–204.

[10] Prakash C, Singh S, Singh M, Verma K, Chaudhary B, Singh S. Multi-objective particle swarm optimization of EDM parameters to deposit HA-coating on biodegradable Mg-alloy. Vacuum 2018;158:180–90.
[11] Prakash C, Singh S, Pabla BS, Sidhu SS, Uddin MS. Bio-inspired low elastic biodegradable Mg-Zn-Mn-Si-HA alloy fabricated by spark plasma sintering. Mater Manuf Process 2019;34(4):357–68.
[12] C. Prakash, H.K. Kansal, B.S. Pabla, S. Puri. To optimize the surface roughness and microhardness of β-Ti alloy in PMEDM process using Non-dominated Sorting Genetic Algorithm-II. In 2015 2nd International Conference on Recent Advances in Engineering & Computational Sciences (RAECS) (pp. 1-6). IEEE.
[13] Prakash C, Singh S, Singh M, Gupta MK, Mia M, Dhanda A. Multi-objective parametric appraisal of pulsed current gas tungsten arc welding process by using hybrid optimization algorithms. Int J Adv Manuf Technol 2019;101(1-4):1107–23.
[14] Singh S, Singh M, Prakash C, Gupta MK, Mia M, Singh R. Optimization and reliability analysis to improve surface quality and mechanical characteristics of heat-treated fused filament fabricated parts. Int J Adv Manuf Technol 2019;102(5-8):1521–36.
[15] Pramanik A, Islam MN, Basak AK, Dong Y, Littlefair G, Prakash C. Optimizing dimensional accuracy of titanium alloy features produced by wire electrical discharge machining. Mater Manuf Process 2019:1–8.
[16] Prakash C, Singh S, Singh M, Antil P, Aliyu AAA, Abdul-Rani AM, et al. Multi-objective optimization of MWCNT mixed electric discharge machining of Al–30SiC p MMC using particle swarm optimization. In: In futuristic composites. Singapore: Springer; 2018. p. 145–64.
[17] Antil P, Singh S, Singh S, Prakash C, Pruncu CI. Metaheuristic approach in machinability evaluation of silicon carbide particle/glass fiber–reinforced polymer matrix composites during electrochemical discharge machining process. Meas Control 2019. DOI:0020294019858216.
[18] Gupta MK, Sood PK, Sharma VS. Machining parameters optimization of titanium alloy using response surface methodology and particle swarm optimization under minimum-quantity lubrication environment. Mater Manuf Process 2016;31:1671–82.
[19] Gupta MK, Sood PK, Sharma VS. Optimization of machining parameters and cutting fluids during nano-fluid based minimum quantity lubrication turning of titanium alloy by using evolutionary techniques. J Clean Prod 2016;135:1276–88.
[20] Hasanipanah M, Danial A, Hassan JA, Muhd-Zaimi AM, Mahmood MDT. Application of PSO to develop a powerful equation for prediction of flyrock due to blasting. Neural Comput Appl 2017;28:1043–50.
[21] Yusup N, Azlan MZ, Siti ZMH. Overview of PSO for optimizing process parameters of machining. Procedia Eng 2012;29:914–23.
[22] Župerl U, Franci C, Gečevska V. Optimization of the characteristic parameters in milling using the pso evaluation technique. Strojniški vestnik-Journal of Mechanical Engineering 2007;53:354–68.
[23] Pan X, Limiao X, Ruixiang L. A new and efficient firefly algorithm for numerical optimization problems. Neural Comput Appl 2018, http://dx.doi.org/10.1007/s00521-018-3449-6.
[24] Karagöz S, Ali RY. A comparison of recent metaheuristic algorithms for crashworthiness optimisation of vehicle thin-walled tubes considering sheet metal forming effects. Int J Veh Des 2017;73:179–88.
[25] Pršić D, Novak N, Vladimir S. A nature inspired optimal control of pneumatic-driven parallel robot platform. Proc Inst Mech Eng Part C J Mech Eng Sci 2017;231:59–71.
[26] Singh G, Walia B. Performance evaluation of nature-inspired algorithms for the design of bored pile foundation by artificial neural networks. Neural Comput Appl 2017;28:289–98.
[27] Aydilek IB. A hybrid firefly and particle swarm optimization algorithm for computationally expensive numerical problems. Appl Soft Comput 2018;66:232–49.
[28] Majumder AAD, Das PK. A standard deviation based firefly algorithm for multi-objective optimization of WEDM process during machining of Indian RAFM steel. Neural Comput Appl 2018;29:665–77.
[29] Abdullah A, Safaai D, Mohd SM, SM ZMH. A new hybrid firefly algorithm for complex and nonlinear problem. In: In distributed computing and artificial intelligence. Berlin, Heidelberg: Springer; 2012. p. 673–80.
[30] Ciurana J, Arias G, Ozel T. Neural network modeling and particle swarm optimization (PSO) of process parameters in pulsed laser micromachining of hardened AISI H13 steel. Mater Manuf Process 2009;24:358–68.
[31] Gopalsamy BM, Biswanath M, Ghosh S. Optimisation of machining parameters for hard machining: grey relational theory approach and ANOVA. Int J Adv Manuf Technol 2009;45:1068.
[32] Pusavec F, Deshpande A, Yang S, M'Saoubi R, Kopac J, Oscar WD, et al. Sustainable machining of high temperature Nickel alloy–inconel 718: part 1–predictive performance models. J Clean Prod 2014;81:255–69.
[33] Tamang SR, Chandrasekaran M. Integrated optimization methodology for intelligent machining of inconel 825 and its shop-floor application. J Braz Soc Mech Sci Eng 2017;39:865–77.
[34] Tripathy M, Mishra S. Bacteria foraging-based solution to optimize both real power loss and voltage stability limit. Ieee Trans Power Syst 2007;22:240–8.
[35] Xu G, Yang Z. Multiobjective optimization of process parameters for plastic injection molding via soft computing and grey correlation analysis. Int J Adv Manuf Technol 2015;78:525–36.
[36] Chauhan P, Pant M, Deep K. Parameter optimization of multi-pass turning using chaotic PSO. Int J Mach Learn Cybern 2015;6:319–37.